Acta Crystallographica Section B
Structural Science
ISSN 0108-7681

Structure solution of the new titanate $Li_4Ti_8Ni_3O_{21}$ using precession electron diffraction

Mauro Gemmi,[a,b]* Holger Klein,[b] Amelie Rageau,[b] Pierre Strobel[b] and Federic Le Cras[c]

[a]Dipartimento di Scienze della Terra 'Ardito Desio' Università degli Studi di Milano, Via Botticelli 23, 20133 Milano, Italy, [b]Institut Neel, Université Joseph Fourier and CNRS, 25 av. des Martyrs, BP 166, 38042 Grenoble CEDEX 9, France, and [c]DRT/LITEN/LT2N, CEA-Grenoble, 17 av. des Martyrs, 38054 Grenoble CEDEX 9, France

Correspondence e-mail: mauro.gemmi@unimi.it

Received 12 October 2009
Accepted 3 November 2009

A sample having stoichiometry $Li[Ti_{1.5}Ni_{0.5}]O_4$ has been synthesized to obtain a spinel structure. The resulting crystalline powder revealed a multiphase nature with spinel as the minor phase. The main phase is a new trigonal phase having a = 5.05910 (1), c = 32.5371 (1) Å. The structure has been solved by direct methods working on a three-dimensional set of intensities obtained from a precession electron-diffraction experiment, and refined on synchrotron powder diffraction data in the space group $P\bar{3}c1$. The model consists of hexagonal layers of edge-sharing octahedra occupied either by the heavy cations Ti and Ni, or preferentially by Li. On the basis of cation-site occupancies the stoichiometry becomes $Li_4Ti_8Ni_3O_{21}$, which is compatible with the microanalysis results.

1. Introduction

The spinel structure, AB_2X_4, is known to accommodate a large range of cations A and B, including Li, Mg and all 3d transition metals with oxidation states mostly +2 to +4. This system has been widely studied for lithium battery materials, especially the manganese oxide spinel $LiMn_2O_4$, where the A-site occupation can be reversibly varied by electrochemical or chemical lithium insertion/extraction (Thackeray, 1997). This stoichiometry change is accompanied by a variation in manganese oxidation state, that functions well because both Mn^{3+} and Mn^{4+} fit well in the octahedral B site of the spinel structure.

Manganese can be partially replaced by Ni^{2+} as in the formula $Li[Mn_{1.5}Ni_{0.5}]O_4$, where all manganese is now tetravalent. Several interesting features occur in this material: firstly, the B cations Ni^{2+} and Mn^{4+} order and form a superstructure of the spinel structure with space group $P4_332$ rather than $Fd\bar{3}m$ (Strobel *et al.*, 2003); secondly, the electrochemical behavior is strongly modified and characterized by the appearance of a redox plateau at 4.8 V *versus* Li–Li^+ (Kawai *et al.*, 1999). This makes this material attractive for battery applications because of the higher specific energy associated with its high potential. Detailed studies of the electrochemical redox mechanism in $Li[Mn_{1.5}Ni_{0.5}]O_4$, especially by X-ray absorption techniques (Terada *et al.*, 2001), showed that the active redox couple is Ni^{2+}/Ni^{4+} and not the Mn^{3+}/Mn^{4+} couple. Therefore, manganese appears to be 'inert' from the redox point of view and such a high voltage could be expected to occur in other $Li[B^{4+}_{1.5}Ni_{0.5}]O_4$ spinels.

The most obvious choice for an alternative B^{4+} cation is titanium, which is quite compatible with the spinel structure. However, the corresponding titanate, '$Li[Ti_{1.5}Ni_{0.5}]O_4$', has never been reported, in spite of the fact that other titanates of

© 2010 International Union of Crystallography
Printed in Singapore – all rights reserved

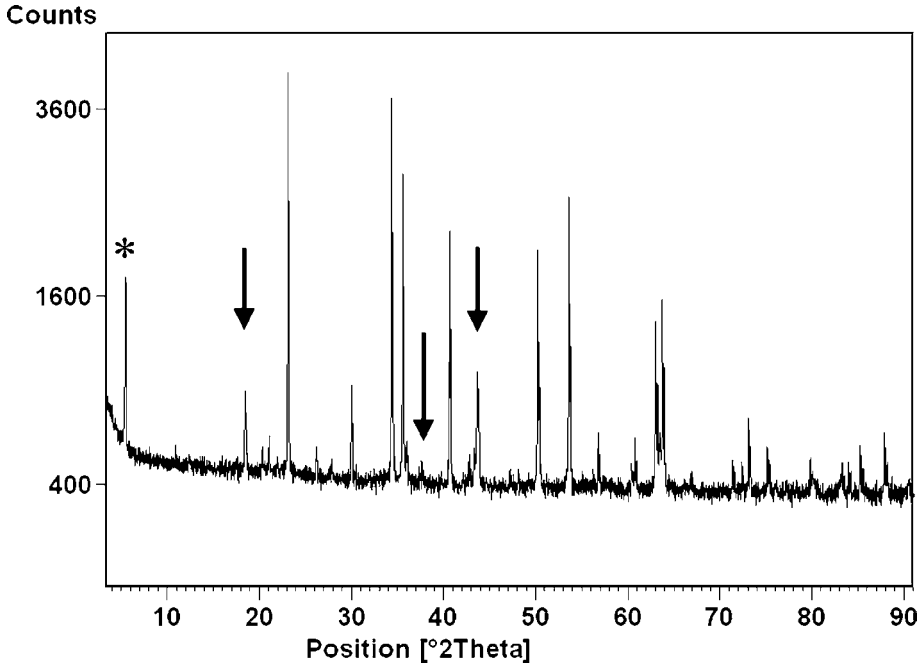

Figure 1
X-ray laboratory powder diffraction pattern. The arrows indicate the peaks compatible with a spinel structure. The asterisk indicates the strong peak with a *d* spacing of 16.2 Å.

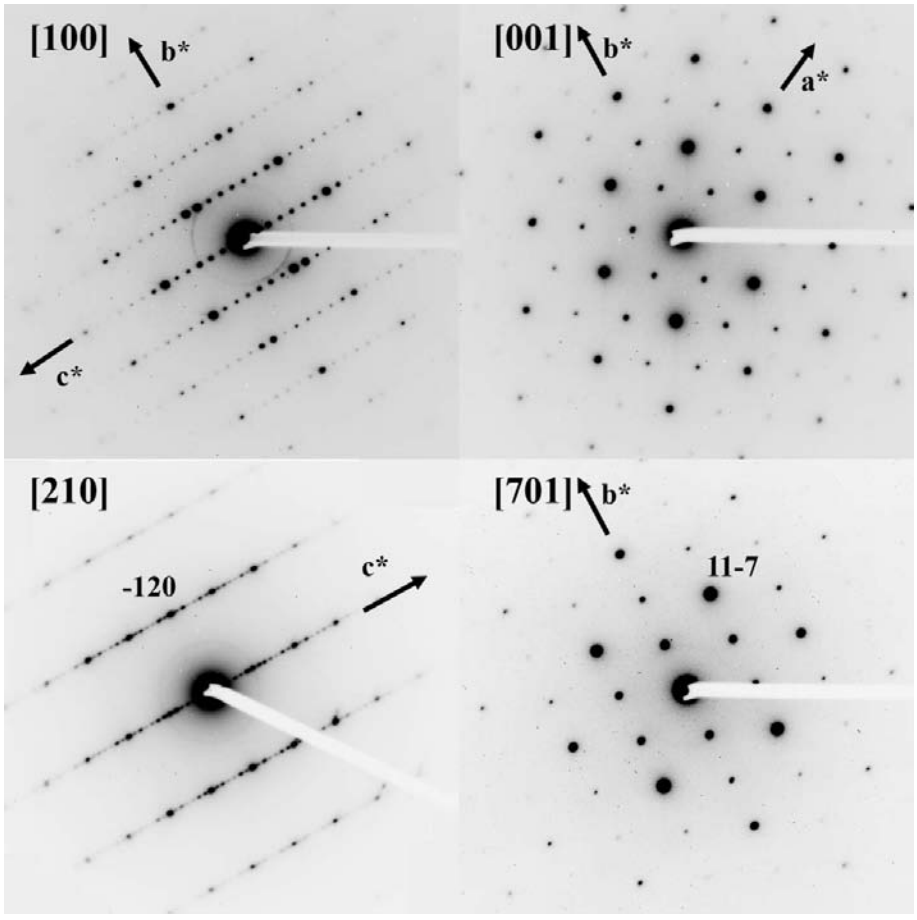

Figure 2
Four main zone axes of the trigonal phase collected in conventional selected-area electron-diffraction mode.

this family, namely $Li[Ti_{1.5}M_{0.5}]O_4$, with M = Mg, Co and Zn, have been described (Kawai *et al.*, 1998).

In the course of attempts to synthesize '$Li[Ti_{1.5}Ni_{0.5}]O_4$', we obtained products presenting X-ray diffraction diagrams featuring a main phase bearing no resemblance to the spinel structure. The aim of the present work is to determine the crystal structure of the new phase obtained from the stoichiometry '$Li[Ti_{1.5}Ni_{0.5}]O_4$' (or '$Li_2Ti_3NiO_8$'). In view of the multiphase character of the samples and of the unavailability of single crystals, this problem is addressed here using synchrotron powder diffraction and electron crystallography.

2. Experimental

2.1. Synthesis

A mixture of Li_2CO_3, Ni acetate and TiO_2 having the cation ratio Li:Ti:Ni equal to 2:3:1 was heated in a Pt crucible at 973 K in air for 24 h. The resulting compound was reground, pelletized and heated at 1173 K in air for 30 h. The last procedure was repeated twice. The product of the synthesis is a light yellow powder.

2.2. Electron microscopy and X-ray diffraction

Transmission electron microscopy was carried out on a Philips CM300ST microscope, at Institut Néel, Grenoble, France, equipped with a Gatan 794 CCD and with a Nanomegas Spinningstar device for performing precession electron diffraction with a tilt up to 4°.

Energy-dispersive spectroscopy (EDS) microanalysis was carried out on a Tecnai F20ST, at the Earth Science Department, University of Milan, Italy, equipped with an EDAX spectrometer.

Laboratory powder X-ray diffraction studies have been carried out on a PANanalytical X'Pert Pro diffractometer equipped with a Cu X-ray tube and an X'Celerator detector.

Synchrotron powder diffraction was carried out at the ID31 and ID09 beamlines of ESRF in Grenoble, France. Data at ID31 were collected in the 2θ range from 1 to 55° with a wavelength of 0.35282 Å. The data reduction was performed with an angular increment of 0.002°. Data at ID09 were collected in the 2θ range from 1 to 30.5° with a wavelength of 0.41465 Å. The angular integration step is 0.0075°.

Rietveld refinement has been carried out using the software *GSAS* (Larson & Von Dreele, 1988).

2.3. Collection and treatment of precessed electron-diffraction data

Precession electron-diffraction patterns have been collected with the CCD camera taking care to avoid CCD saturation. Every pattern has been acquired by summing together several short exposures (normally 5 exposures of 10 s) and checking that the most intense diffraction spot is not saturated. The reflection intensities have been extracted using the software package *QED* (Belletti *et al.*, 2000).

The simulated kinematical electron-diffraction patterns have been generated using the *eMap* simulation software package (Analitex, Sweden).

3. Results

Preliminary powder X-ray diffraction with normal laboratory equipment reveals that the sample is not a spinel single-phase sample. Diffraction peaks characteristic of a spinel phase having $a \simeq 8.36$ Å are present, but the strongest peaks cannot be indexed with the spinel unit cell. In particular, a strong reflection at a small angle showing a periodicity of 16.25 Å indicates that another phase with at least one long unit-cell parameter is present in the sample (Fig. 1). In order to clarify the nature of these phases we investigated the sample using electron diffraction.

3.1. The trigonal phase

Among the first crystals we found in the microscope we observed a pattern containing the 16.25 Å periodicity. Since we considered this as the marker of the main unknown phase, we collected electron-diffraction patterns along the maximum possible number of zone axes on this crystal. The software package *QED* (Belletti *et al.*, 2000) indexed these patterns with a hexagonal cell having $a \simeq 5.0$ and $c \simeq 32.5$ Å. The cell was further checked by indexing patterns taken on different crystals and by checking that the measured angles between the zone axes were compatible with the indexing assigned. It has been possible to index in a consistent way ten different zone axes ([1,0,0], [0,0,1], [2,1,0], [3,1,0], [7,0,1], [10,0,1], [14,0,1], [10,−10,1], [17,−10,1], [24,−10,1]) taken on several different crystals. Some of these patterns are displayed in Fig. 2. The [001] zone axis is compatible with a three- or sixfold axis, while the [100] zone axis does not show an *mm* symmetry, therefore the crystal system must be trigonal. The only extinction conditions are $h0l$, $l = 2n$, which are compatible with the space groups $P\bar{3}c1$ and $P3c1$, depending on the presence or absence of an inversion center. In order to determine the Ni:Ti atomic ratio, we performed energy-dispersive microanalysis on several crystals. The average chemical compositions obtained is $Ti_{At\%} = 75\ (2)\%$, $Ni_{At\%} = 25\ (2)\%$, in agreement with the starting chemical composition of the reagents.

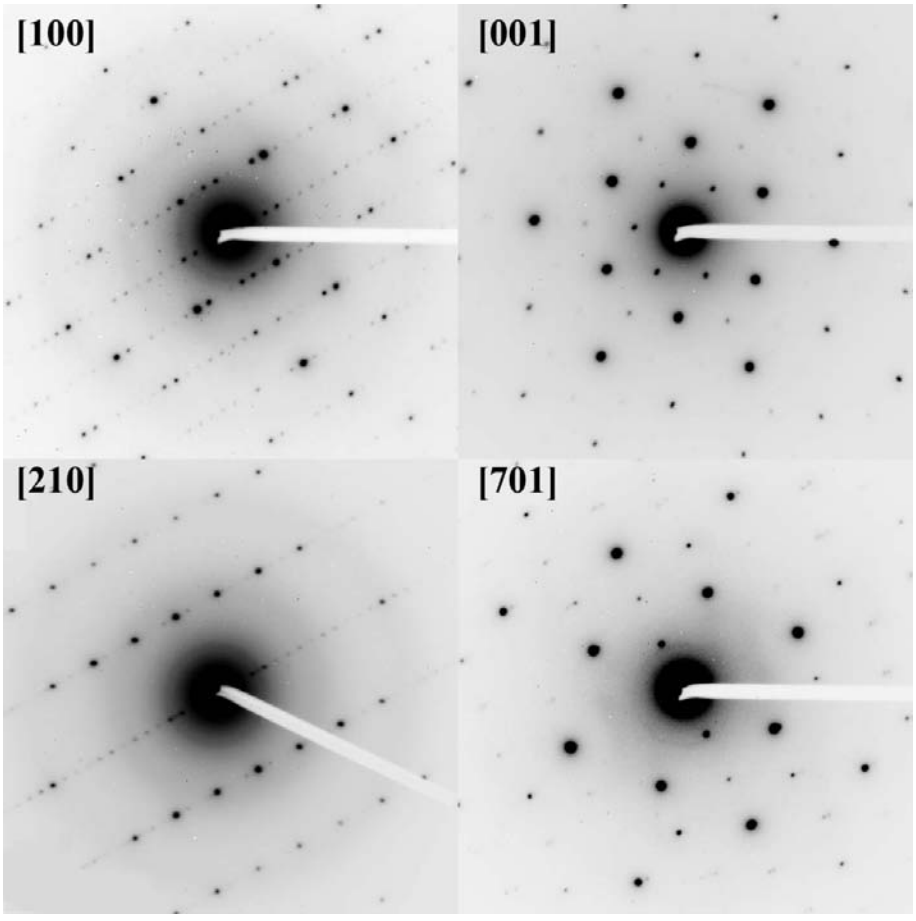

Figure 3
The same zone axes of Fig. 2 but collected in precession electron-diffraction mode. The precession angles are: 3.2° for [100], 3.5° for [001], 2.5° for [210] and 3.5° for [701].

3.2. Structure solution of the trigonal phase

Owing to the presence of more than one phase, we decided to solve the structure of the trigonal phase using precession electron diffrac-

Table 1
Refined unit-cell parameters and atomic position for the $Li_4Ti_8Ni_3O_{21}$ phase.

Space group: $P\bar{3}c1$; unit cell: a = 5.05910 (1), c = 32.5371 (1) Å; unit-cell volume V = 721.202 (2) Å^3; ID31 figure of merit R_p = 0.102, wR_p = 0.164, R_{Bragg} = 0.175; ID09 figure of merit R_p = 0.057, wR_p = 0.109, R_{Bragg} = 0.136.

Atom	x	y	z	Occupancy	U_{iso}
*M*1	0	0	0.15122 (6)	0.898 (17)Ti + 0.102 (17)Ni	0.0045 (1)
*M*2	1/3	2/3	0.21661 (10)	1 Ti	
*M*3	2/3	1/3	0.07793 (6)	0.384 (17)Ti + 0.616 (17)Ni	
*M*4	1/3	2/3	0.00938 (8)	0.823 (15)Ti + 0.177 (15)Ni	
*M*5	0	0	0.06165 (8)	0.924 (6)Ti + 0.076 (6)Li	
*M*6	1/3	2/3	0.13339 (10)	0.548 (4)Ni + 0.452 (4)Li	
Li1	2/3	1/3	0.19373 (24)	0.120 (4)Ni + 0.880 (4)Li	
O1	−0.2949 (14)	0.0061 (15)	0.10547 (16)	1	0.0037 (3)
O2	−0.3764 (20)	0	1/4	1	
O3	−0.3438 (16)	0.7109 (13)	0.17894 (17)	1	
O4	−0.3539 (16)	0.6312 (13)	0.03596 (17)	1	

tion (PED) in order to avoid the problem of reflection overlap, which is inherent to powder diffraction data. Conventional electron diffraction is rarely used for structure solution, since the dynamical diffraction destroys the simple proportional relation between the square modulus of the structure factors and the reflection intensities (Cowley, 1968). However, after the invention of the precession technique by Vincent & Midgley (1994), it has been possible to collect electron-diffraction patterns much closer to kinematical conditions than the usual selected area diffraction. A PED pattern is collected by precessing the electron beam around the optical axis on a conical surface having the vertex fixed on the specimen plane. Since during the precession the pattern is tilted off the zone axis, few reflections are excited at the same time and the multiple scattering between the diffracted beams is strongly reduced. It has been proved that the electron-diffraction intensities collected in this way are suitable for structure solution (Gjønnes *et al.*, 1998; Gemmi *et al.*, 2003; Dorset, 2006; Own *et al.*, 2006; Weirich *et al.*, 2006) and nowadays a commercial device has made the technique available to several laboratories with an obvious increase of scientific results in this field (see Nicolopoulos & Weirich, 2007; Xie *et al.*, 2008; Gilmore *et al.*, 2008; Mugnaioli *et al.*, 2009; Boullay *et al.*, 2009). Some PED patterns collected on the trigonal phase are displayed in Fig. 3 and correspond to the same patterns of Fig. 2, taken on the same crystals.

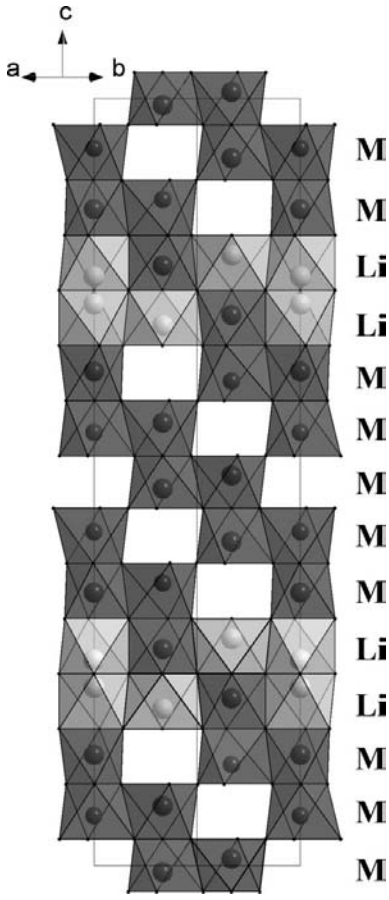

Figure 4
The structural model of the trigonal phase obtained with the precessed electron-diffraction data. The structure is viewed along [110] and only a (110) section is displayed to avoid the superposition of the polyhedra. The layer type is indicated with a label (M or Li), as explained in the text.

To obtain a three-dimensional set of reflection intensities we followed the same procedure outlined in Gemmi & Nicolopoulos (2007). We collected several zone axes with the maximum precession angle compatible with the overlapping of higher-order Laue zones, we integrated the reflection intensities, and we corrected these intensities for precession geometry using the formula

$$I_{corr}(\mathbf{g}) = I_{exp}(\mathbf{g})\left[g\sqrt{1-(g/2R)^2}\right], \qquad (1)$$

where g is the length of the reciprocal vector $\mathbf{g}$ and R is the radius of the Laue circle (Gjønnes, 1997).

After that, we merged the intensities coming from different zone axes using a common row of reflections. The final three-dimensional set was derived using the [100], [210], [310] (merged with the *00l* common reflections), [701], [10,01], [14,01] and [001] (merged with the 0*k*0 common reflections) zone axes, taken with precession angles varying between 2 and 3.4°. The R values of merging vary in the ranges 0.11–0.15 and

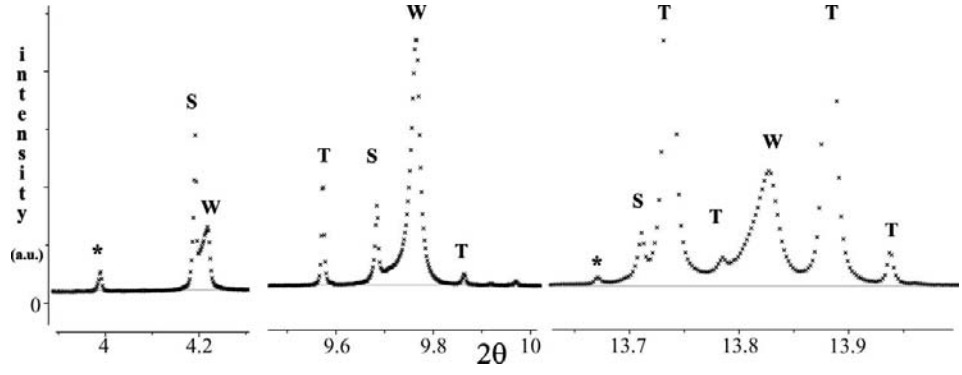

Figure 5
Enlargement of the 2θ ranges containing the three strongest peaks not indexed with the trigonal cell. The peaks belonging to a spinel phase are marked as S. Those belonging to the trigonal phase are marked as T. The peaks labelled as W cannot be indexed either with the spinel or with the trigonal cell and show a wide asymmetric shape. The asterisk indicates other unindexed peaks. The intensity of the strongest W peak in the central interval is 10 times smaller than the intensity of the strongest peak of the trigonal phase. The experimental data are those collected at the ID31 beamline (see Fig. 6 for the entire pattern).

0.04–0.06 for the 00l and 0k0 common rows. The final merged data set contains 349 independent reflections.

For the structure solution we applied conventional direct methods using *SIR*2008, a module of the software package *IL MILIONE* (Burla *et al.*, 2007), with a cut off for high-resolution reflections at 1.2 Å, giving a data set of 105 independent reflections. The internal R values calculated on this data set are: $R_{\rm int}$ = 0.122 for all the reflections and $R_{\rm int}$ = 0.063 if calculated only on the reflections used for the solution.

The structure solution was achieved in both $P\bar{3}c1$ and $P3c1$ space groups, with final R values of 0.285 and 0.266. Both solutions give the same structural model and the small differences between them are beyond the precision that electron data can give. In the case of $P\bar{3}c1$ the asymmetric unit is formed by six heavy cations M (M = Ni, Ti), two Li and four O (see Table 1 of the supplementary material[1]). In $P3c1$ the M and Li positions are doubled and the independent oxygen positions are 7.

The model consists of hexagonal layers of edge-sharing octahedra occupied either by M or Li (Fig. 4). The layers occupied only by M (M layers) are of the corundum type, having 2/3 of the octahedra occupied; those where the Li is present (Li layers) have all the octahedra occupied. As can be easily determined from the picture, the two Li positions generated from the site on the unit-cell edge are too close to each other. Therefore, this position is either an artefact, or it is misplaced and should be closer to the center of the octahedron or it cannot be fully occupied. The unit cell is formed by a double stacking of five M layers, in a corundum-type sequence, and two Li layers for a total of 14 layers (5M–2Li–5M–2Li). Since every M layer contains three O and two M, while every Li layer contains three O, one Li (if we consider the second Li site empty) and one M, the chemical content of the unit cell should be $2M_{12}Li_2O_{21}$. Following the microanalysis results, this gives $Ti_9Ni_3Li_2O_{21}$ as the chemical formula, which violates electroneutrality since we expect to have Ti^{4+} and Ni^{2+}, and is Li-deficient compared with the nominal composition. Therefore, some of the M sites must also be occupied by Li. Unfortunately, the electron data cannot allow any refinement to check this hypothesis.

3.3. Rietveld refinement with synchrotron powder diffraction.

To go further in the structure determination we decided to try a Rietveld refinement. This posed several problems since we did not have any structural model for the other unknown phases.

An indexing of the X-ray powder diffraction pattern indicates, however, that the peaks not belonging to the trigonal phase are in a minority and are weak, suggesting that a Rietveld refinement without taking into account their contribution would still give reliable results.

In order to minimize the peak overlapping between the different phases we collected the data at ID31, a synchrotron high-resolution powder diffraction beamline. The high resolution of these data allows three different sets to be identified among the weak peaks not indexed by the trigonal cell; one set of narrow peaks corresponding to a cubic spinel, one set of broadened peaks that always follows a peak of the spinel phase and a third set of narrow peaks belonging to other unknown phases (Fig. 5). The presence of the spinel phase has also been confirmed by electron diffraction. The spinel has been found to always be intergrown with another phase which is a superstructure of the spinel phase and exhibits strong stacking disorder that could explain the second set of broad X-ray diffraction peaks. The structure investigation of these phases will be the subject of another paper which is currently in preparation (Gemmi *et al.*, 2009).

Unfortunately, problems with the beam stop position partially masked the diffraction pattern at low scattering angles so that the intensity of the 002 peak, the first reflection of the trigonal phase, was underestimated. The low scattering-angle data are quite important to evaluate the site occupancies, since it is in this scattering range that the scattering factors of different chemical species are most different. Therefore, we decided to perform a simultaneous refinement on two data sets: the one collected at ID31 excluding the low scattering angles, and another collected at ID09 without underestimation of the low scattering region.

The strategy of the refinement was the following. We tried first the centrosymmetric space group $P\bar{3}c1$, using the

[1] Supplementary data for this paper are available from the IUCr electronic archives (Reference: DR5025). Services for accessing these data are described at the back of the journal.

coordinates given by *SIR*2008 as the starting point (see Table 1 of the supplementary material). We added, as a second phase, a cubic spinel with Li in the tetrahedral site, and Ti and Ni in the octahedral site. As overall parameters we refined the scale factors of each histogram; 20 and 10 coefficients of a Chebichev polynomial curve for the background of the ID31 and ID09 pattern; lattice parameters and zero shift; three parameters to model the full width at half-maximum of the pseudo-Voigt profile function (one for the Gaussian and two for the Lorentian contribution, *i.e.* GW, LX and LY of *GSAS* coding). As structural parameters we refined the atomic coordinates of all the atoms, one common displacement parameter for the cation sites and one for the oxygen sites. We considered the *M* sites as occupied by both Ti and Ni and we refined their occupancy. We did not consider the second Li site (half occupied) in the refinement. After a preliminary refinement we found that:

(i) Two of the *M* sites (*M*4 and *M*5) cannot be fully occupied by Ti and Ni, their occupancies refine to 0.90 and 0.60. Moreover, their large average *M*—O distances suggest possible Li substitutions.

(ii) The Li1 site requires more electron density than just one Li atom.

By taking into account the constraints given by the chemical composition (Ti:Ni $\simeq$ 3) and the average cation–oxygen distances (*M*4 smaller than *M*5), we considered *M*4 as occupied by Ti and Li, and *M*5 and Li1 occupied by Ni and Li. Each occupancy of these sites was constrained to 1 during the refinement, since without this constraint the refinement converges to negative occupancies.

The result of the final refinement is reported in Table 1 and the fit of the ID31 and ID09 patterns are displayed in Fig. 6. In order to have an idea of how kinematical the PED patterns are, a kinematical simulation of the same zone axes of Figs. 2 and 3 is displayed in Fig. 7. A very close resemblance to the PED patterns (but not to the SAED patterns) is observed.

Any refinement using the non-centrosymmetric space group *P*3*c*1 gave strong correlation problems and it was not possible to reach a final stable solution.

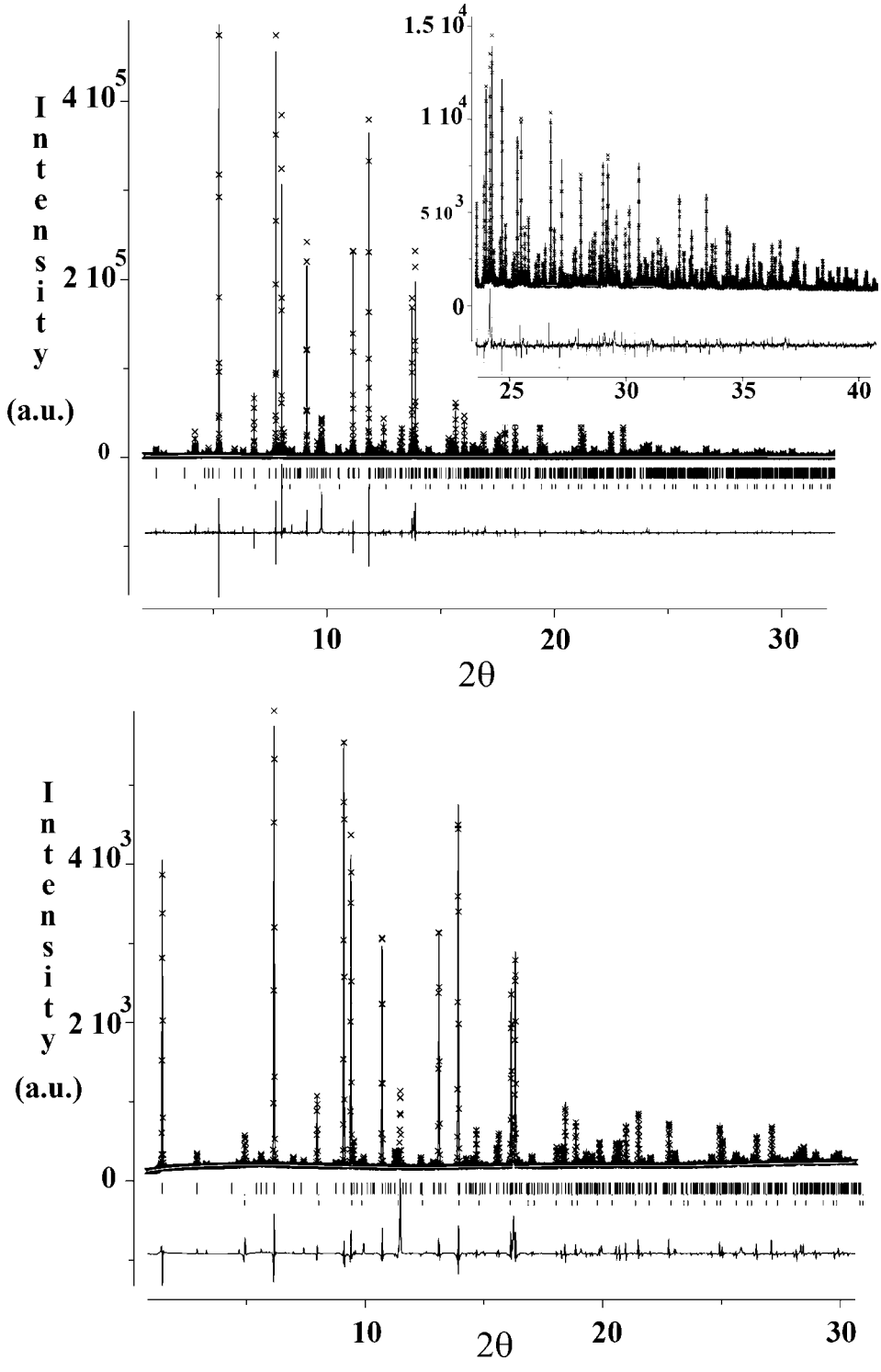

Figure 6
Results of the Rietveld refinement of the $Li_4Ti_8Ni_3O_{21}$ structure on the synchrotron powder diffaction data taken at ID31 (top) and ID09 (bottom). In the ID31 data, the box at the right reports the fit for the high 2θ angles.

Table 2
List of the cation–oxygen distances and the bond valences.

Bond valences are calculated according to Brown & Altermatt (1985).

Atom 1	Atom 2	Distance (Å)	Average distance (Å)	Charge	Bond valence
*M*1	O1	2.119 (5)	1.99	3.8	3.88
	O3	1.853 (8)			
*M*2	O2	1.925 (10)	1.95	4	4.24
	O3	1.964 (5)			
*M*3	O1	1.976 (4)	2.03	2.76	2.68
	O4	2.074 (5)			
*M*4	O4	1.889 (8)	2.02	3.64	3.45
	O4	2.148 (5)			
*M*5	O1	2.075 (5)	2.04	3.76	3.09
	O4	2.011 (8)			
*M*6	O1	2.020 (7)	2.08	1.55	1.58
	O3	2.133 (5)			
Li1	O2	2.427 (6)	2.21	1.12	1.02
	O3	1.995 (8)			
O1				−2	−1.7
O2				−2	−1.65
O3				−2	−2.03
O4				−2	−2.09

Table 3
List of the cation–cation distances.

The terms face and edge indicate that the two cations are centering two octahedra sharing a face or an edge.

Atom 1	Atom 2	Distance (Å)
*M*1	*M*5 face	2.914 (3)
	*M*6 edge	2.978 (1)
*M*2	*M*6 face	2.708 (5)
	Li1 face	2.921 (8)
	Li1 edge	3.015 (2)
*M*3	*M*4 face	2.841 (3)
	*M*5 edge	2.968 (1)
*M*4	*M*4 edge	2.984 (1)
Li1	*M*1 none	3.230 (3)

4. Discussion

The refined structure is displayed in Fig. 8. Four cation sites are preferentially occupied by Ti (*M*1, *M*2, *M*4, *M*5), two have a large Ni content (*M*3, *M*6) and one is mainly occupied by Li (Li1). Li is also present in the *M*5 and *M*6 sites. The cation–oxygen distances are in agreement with the occupancy of the sites. *M*2, which is only occupied by Ti, shows the smallest average cation–oxygen distance, while the sites containing Li have an average cation–oxygen distance that increases with the Li content (see Table 2).

The Ti is distributed in order to minimize the strong repulsion between the centering octahedra of the cations that share faces. The octahedra preferentially occupied by Ti in fact never share a face. The repulsion across the shared octahedral faces is compensated by a displacement of the cation towards the vacant sites (see Table 3). The only site for which that is impossible, *M*2, has the less distorted octahedral coordination. The Li1 site is the most distorted, it approaches a triangular coordination with Li1—O2 = 1.99 Å and with three much longer Li1—O3 = 2.42 Å. A similar coordination, slightly more distorted has already been observed in $Li_2Ti_3O_7$ (Bordet *et al.*, 2000), and empirical bond-valence calculations give a reasonable valence for Li1 (see Table 2). The stoichiometry according to the refined occupancies is $Li_{2.81}Ti_{8.04}Ni_{3.14}O_{21}$. In this stoichiometry one positive charge is missing. The strong underbonding of O1, O2 suggests that this missing

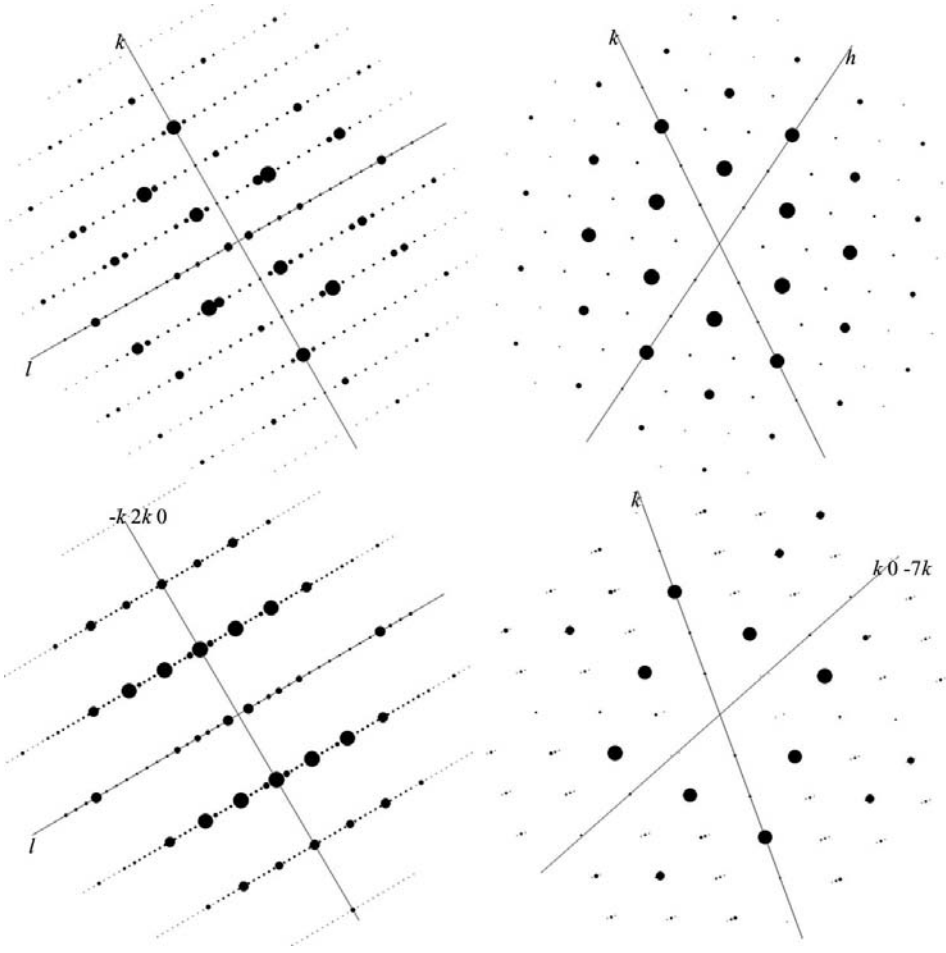

Figure 7
Kinematical simulation of the patterns shown in Figs. 2 and 3. The simulation was carried out with the software eMap of Analitex, Sweden, using the refined model as the structural model.

charge is due to Li occupying the second Li site obtained in the electron-diffraction solution, and the two vacant octahedral sites bonded to O1. Some Li can also go in the *M*4 site, which has a charge higher than that predicted by bond valence, and also shows quite a long *M*—O4 distance (2.15 Å) for a Ti–Ni site. The *M*5 site shows the same discrepancy between charge and bond valence, however, in this case we believe that it is due to Li–Ni–Ti mixed occupancy, which is impossible to estimate correctly. The correct stoichiometry should be $Li_4Ti_8Ni_3O_{21}$, that in terms of Ni and Ti atomic percentages gives TiAt% = 73%, NiAt% = 27%, values that are in agreement with the microanalysis results.

Long stacking of hexagonal octahedral layers is not new for oxides containing Li, Ni and Ti (see Fig. 9). The hexagonal $Li_2Ti_3O_7$ has a *c* axis of 69.9 Å corresponding to a stacking of 30 layers of corundum $[Ti_2O_3]^{2+}$-type and $LiNbO_3$-type (Bordet *et al.*, 2000), $Li_xNi_{1-y}Ti_yO_2$ $(0.1 \leq y \leq 0.3)$ is isostructural with $LiNiO_2$, with a *c* axis of 14.2 Å corresponding to an alternate stacking of fully occupied octahedral layers of Li and (Ni,Ti) for a total of six layers per unit cell (Chang *et al.*, 1996). Evidence of a similar structure for $LiNi_{0.5}Ti_{0.5}O_2$ has been reported by Tsuda *et al.* (2005). By checking in the ICDS database we discovered that the oxide $Mn_{11}Ta_4O_{21}$ has a similar unit cell ($a = 5.378$, $c = 34.04$ Å) with the same space group $P\bar{3}c1$ as our new structure (Grins & Tyutyunnik, 1998). This structure in fact results from the stacking of 14 octahedral layers, as in this case but the stacking is different.

As can be seen both by discrepancies between the expected charge and bond valences and by the high *R* values of the Rietveld fit, the refined structure of $Li_4Ti_8Ni_3O_{21}$ could be just an average model. This is because the powder diffraction data are perturbed by the presence of other phases, whose structural model is unknown, and by possible polytypism of the trigonal phase. Very rarely have we observed the presence of $0, 2n+1, l$ reflections in the [100] diffraction patterns, which are forbidden by the space-group symmetry and cannot be switched on by dynamical diffraction in the [100] zone axis (Fig. 10).

5. Conclusions

Precession electron diffraction opens the possibility of building reliable structural models of unknown phases in multiphase powder samples when X-ray powder diffraction suffers a lack of three-dimensional information. This paper is an example of how to couple the two techniques together. Precession electron diffraction is crucial to identify the synthesized phases and to obtain the starting model of those

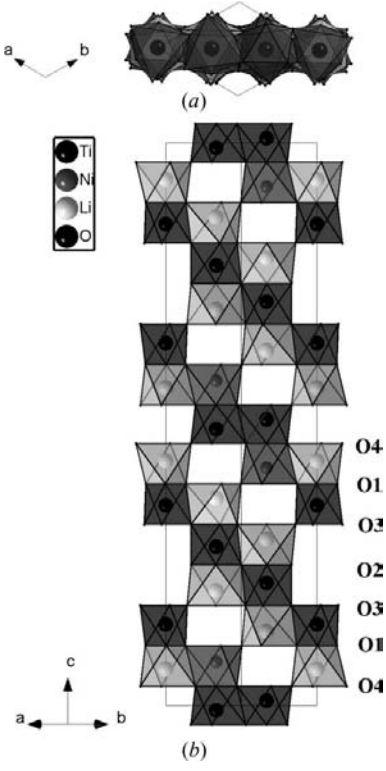

Figure 8
Structure of $Li_4Ti_8Ni_3O_{21}$ obtained from the Rietveld refinement. For a clearer representation a (110) section is displayed in (*a*) the [001] projection and (*b*) viewed along its normal. The dark grey octahedra are those mainly occupied by Ti. The light grey octahedra are those preferentially occupied by Ni and the white octahedra are those that have a mixed occupancy with Li and another Ni or Ti cation. The labels of the oxygen forming the layers are reported on the right.

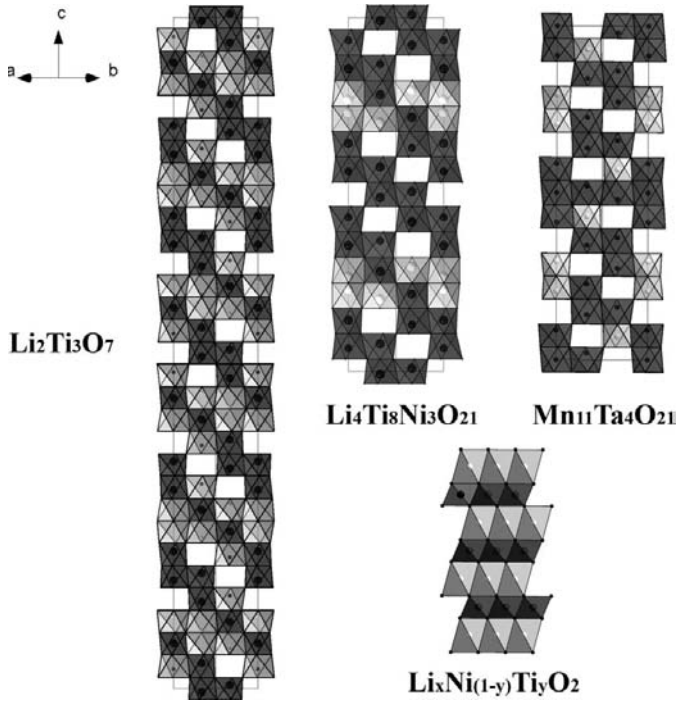

Figure 9
Comparison between the structure of $Li_4Ti_8Ni_3O_{21}$ solved with precessed electron-diffraction data and other Li, Ni, Ti oxides showing the same structural motif of stacked octahedral layers.The dark polyhedra are those occupied by heavy cations (Ni or Ti), the light polyhedra are those containing Li. The $Ta_4Mn_{11}O_{21}$ oxide is reported since it has a very similar unit cell and the same space group as our compound, but a different structure. The Ta polyhedra are light and the Mn polyhedra are dark.

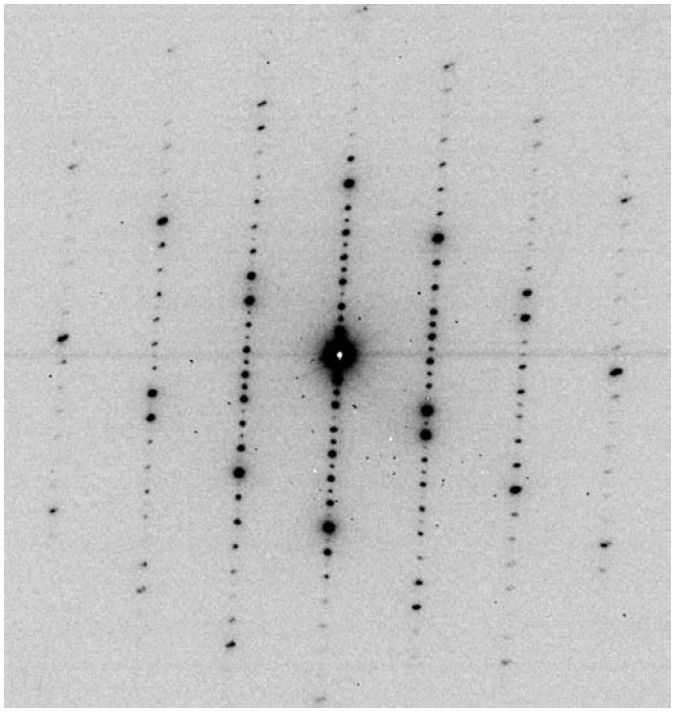

Figure 10
Selected-area diffraction pattern oriented in the [100] zone axis that shows the presence of the $0, 2n + 1, l$ forbidden reflections (*cf.* the same zone axis displayed in Fig. 2).

unknown. X-ray powder diffraction allows the model to be completed and refined. By this complementary approach we solved and refined the structure of the new unknown $Li_4Ti_8Ni_3O_{21}$ phase. Since this is the main phase of the synthesis the Rietveld refinement converges, even though some minor unknown phases are not considered. However, for samples where the unknown phase is not the only major phase, the structural model derived with PED can still be checked with Rietveld refinement provided we have a structural model for all the other major phases. In this case it would be difficult to refine the model. Nevertheless, its knowledge would furnish a possible chemical composition and consequently a way to tune the chemical synthesis for obtaining the unknown phase as the dominant one.

PED has revealed a remarkable sensitivity to determining the light atom positions and to label them correctly. In the solution obtained with PED data the atomic positions are slightly misplaced from those refined with the Rietveld method, but each atom has been assigned with its correct atomic species apart from the ratio of the Ti:Ni occupancy, which was not estimated. The two sites labeled as Li are those that, according to Rietveld refinement, must have the highest Li content. This demonstrates that PED approaches kinematical diffraction and must be considered an alternative structure solution technique to support X-ray powder diffraction.

The authors would like to thank Michela Brunelli and Marco Merlini for collecting the diffraction data on ID31 and ID09 respectively, and Gunnar Svensson for pointing out the similarity of the $Li_4Ti_8Ni_3O_{21}$ structure with the $Ta_4Mn_{11}O_{21}$ structure.

References

Belletti, D., Calestani, G., Gemmi, M. & Migliori, A. (2000). *Ultramicroscopy*, **81**, 57–65.
Bordet, P., Bougerol Chaillout, C., Grey, I. E., Hodeau, J. L. & Isnard, O. (2000). *J. Solid State Chem.* **152**, 546–553.
Boullay, P., Dorcet, V., Pérez, O., Grygiel, C., Pellier, W., Mercey, B. & Hervieu, M. (2009). *Phys. Rev. B*, **79**, 184108.
Brown, I. D. & Altermatt, D. (1985). *Acta Cryst.* B**41**, 244–247.
Burla, M. C., Caliandro, R., Camalli, M., Carrozzini, B., Cascarano, G. L., De Caro, L., Giacovazzo, C., Polidori, G., Siliqi, D. & Spagna, R. (2007). *J. Appl. Cryst.* **40**, 609–613.
Chang, S. H., Kang, S., Song, S., Yoon, J. & Choy, J. (1996). *Solid State Ionics*, **86–88**, 171–175.
Cowley, J. M. (1968). *Prog. Mater. Sci.* **13**, 267–321.
Dorset, L. D. (2006). *Z. Kristallogr.* **221**, 260–265.
Gemmi, M., Klein, H., Rageau, A., Strobel, P. & Le Cras, F. (2009). *J. Solid State Chem.* In preparation.
Gemmi, M. & Nicolopoulos, S. (2007). *Ultramicroscopy*, **107**, 483–494.
Gemmi, M., Zou, X. D., Hovmöller, S., Migliori, A., Vennström, M. & Andersson, Y. (2003). *Acta Cryst.* A**59**, 117–126.
Gilmore, C. J., Dong, W. & Dorset, D. L. (2008). *Acta Cryst.* A**64**, 284–294.
Gjønnes, K. (1997). *Ultramicroscopy*, **69**, 1–11.
Gjønnes, J., Hansen, V., Berg, B. S., Runde, P., Cheng, Y. F., Gjønnes, K., Dorset, D. L. & Gilmore, C. J. (1998). *Acta Cryst.* A**54**, 306–319.
Grins, J. & Tyutyunnik, A. (1998). *J. Solid State Chem.* **137**, 276–282.
Kawai, H., Nagata, M., Tukamoto, H. & West, A. R. (1999). *J. Power Sources*, **81–82**, 67–72.
Kawai, H., Tabuchi, M., Nagata, M., Tukamoto, H. & West, A. R. (1998). *J. Mater. Chem.* **8**, 1273–1280.
Larson, A. C. & Von Dreele, R. B. (1988). *GSAS.* Report LAUR 86–748. Los Alamos National Laboratory, New Mexico, USA.
Mugnaioli, E., Gorelik, T. & Kolb, U. (2009). *Ultramicroscopy*, **109**, 758–765.
Nicolopoulos, S. & Weirich, T. (2007). Editors. *Proceedings of the Electron Crystallography School* 2005, ELCRYST 2005: New Frontiers in Electron Crystallography, Vol. 107, pp. 431–558. Amsterdam: Elsevier.
Own, C. S., Sinkler, W. & Marks, L. D. (2006). *Ultramicroscopy*, **106**, 114–122.
Strobel, P., Ibarra-Palos, A., Anne, M., Poinsignon, C. & Crisci, A. (2003). *Solid State Sci.* **5**, 1009–1018.
Terada, Y., Yasaka, K., Nishikawa, F., Konishi, T., Yoshio, M. & Nakai, I. (2001). *J. Solid State Chem.* **156**, 286–291.
Thackeray, M. M. (1997). *Prog. Solid State Chem.* **25**, 1–71.
Tsuda, M., Arai, H., Takahashi, M., Ohtsuka, H., Sakuray, Y., Sumitomo, K. & Kageshima, H. (2005). *J. Power Sources*, **114**, 183–190.
Vincent, R. & Midgley, P. A. (1994). *Ultramicroscopy*, **53**, 271–282.
Weirich, T., Portillo, J., Cox, G., Hibst, H. & Nicolopoulos, S. (2006). *Ultramicroscopy*, **106**, 164–175.
Xie, D., Baerlocher, C. & McCusker, L. B. (2008). *J. Appl. Cryst.* **41**, 1115–1121.